Vision, Modeling, and Visualization (2017)
M. Hullin, N.N. (Eds.)

Finite Time Steady Vector Field Topology - Theoretical Foundation and 3D Case -

Anke Friederici [1], Tobias Günther [2], Christian Rössl [1] and Holger Theisel [1]

[1] University of Magdeburg, Germany [2] ETH Zurich, Switzerland

Abstract

Vector Field Topology is the standard approach for the analysis of asymptotic particle behavior in a vector field flow: A topological skeleton is separating the flow into regions by the movement of massless particles for an integration time converging to infinity. In some use cases however only a finite integration time is feasible. To this end, the idea of a topological skeleton with an augmented finite-time separation measure was introduced for 2D vector fields. We lay the theoretical foundation for that method and extend it to 3D vector fields. From the observation of steady vector fields in a temporal context we show the Galilean invariance of Vector Field Topology. In addition, we present a set of possible visualizations for finite-time topology on 3D topological skeletons.

1. Introduction

One widely used approach to visualize a steady vector field is representing the flow through areas of similar asymptotic behavior. This allows for a quick overview of the fields structure and is the basis for a number of techniques. Vector Field Topology extracts such a skeleton: separatrices are integrated from critical points and boundary switch points. They form lines or surfaces, respectively, segmenting the flow into regions with the same asymptotic behavior. This simple method has several appealing aspects. Most prominently, only few points in the domain need to be considered for a complete segmentation, resulting in few primitives to be visualized, overall requiring little computational effort.

In unsteady vector fields, a straightforward application of Vector Field Topology is generally not possible, as the domain is restricted in the time dimension. The asymptotic behavior can thus only be approximated in a finite time frame. Generally, the flow map has to be densely sampled and integrated in the whole domain to extract a segmentation, commonly Lagrangian Coherent Structures (LCS). Several methods have been introduced for their computation. Most prominent among them is the extraction of ridge lines in the Finite-Time Lyapunov Exponent (FTLE) field.

Another approach to a definition of topology in unsteady flow is a reduction to a steady flow field by substracting a certain unsteady flow field [BPKB14, WGS07]. Instead of a costly LCS extraction, now the much cheaper Vector Field Topology can be computed. While Vector Field Topology is applicable to the generated field in practice, the resulting skeleton captures the behavior for integrations times converging to infinity, outside the finite time frame of the original data.

In this paper, we extend and theoretically consolidate the previous work [FRT15]. Basically, we compute a local measure of separation relative to the asymptotic separation. However, we can simplify the method to finite-time computations only. The measure is therefor cheap to compute and may safely be applied to vector fields only defined in a certain time frame.

More specifically, we segment the on flow segmentations based on finite integration behavior within steady fields. In chapter 3 it will be shown that this skeleton is equivalent to Lagrangian Coherent Structures of steady fields and therefor linked to maxima of flow separation. On the separating structures, the separation accumulated over a finite integration time is compared against the final separation at the saddle.

In this work, we argue that the separating structures in steady fields coincide with the Vector Field Topology, even for finite integration times. To that end, we define *path line topology* by observing steady Vector Field behavior in an unsteady domain. Additionally, we extend both computation and visualization to 3D steady fields and apply different rendering techniques to tackle the problem of surface occlusion.

2. Related Work

The general frame of Vector Field Topology [HH89] and several extensions [SKMR98, dLvL99a, WS01] have been the basis to many further works. The 3D variant contains separatrix planes in addition

to lines, while generally the same topological structures are extracted [GLL91, HH91, MBHJ03, MBS*04, TWHS03, WTHS04a]. As the general behavior is captured in a small number of structures, it has been utilized for the simplification, smoothing and compressing of steady vector fields [dLvL99a, dLvL99b, TSH00, TSH01, WJE01, LRR00, SLR03, TRS03], and vice versa the construction of such [The02, WTHS04b]. For a more detailed discussion, we refer to the overviews presented in [LHZP07, PPF*11, WWL16, HLH*16].

A simple application of topology to unsteady vector fields is unfortunately not possible. When the integration time is bounded, asymptotic behavior cannot be analyzed. Instead, other measures of similarity or difference have to be found for the partition of a domain. Most commonly, Lagrangian Coherent Structures (LCS) are extracted from the flow and define the boundaries between areas. Several methods exist to extract these structures. A widely used variant is the computation of the Finite-Time Lyapunov Exponent (FTLE) [Hal01, HY00] for every point in the domain. LCS coincide with ridges in the resulting scalar field, though the extraction of exact ridge lines is cumbersome. A number of extensions to FTLE have been proposed. The high correlation between shear flow and high FTLE values has been tackled by [PPF*12]. Performance and quality were improved by several works [GKT16, GGSLHH09, GGTH07, SP09, SP07, SRP11, LM10] and FTLE ridges have found a broad spectrum of applications [Hal02, LCM*05, SLP*09, WPJ*08]. As their convergence to material structures has be proven [SLM05], they can be used to describe the topology of unsteady vector fields [SW10, USE13].

To circumvent the computational cost of LCS methods, another approach recurring in unsteady vector field analysis is the decomposition of the field by subtracting a background flow [BPKB14, WGS07]. When the behavior of the data can be captured in a steady part, Vector Field Topology can be applied to efficiently compute separating structures. In this situations, a finite-time evaluation of separation is preferable to an analysis of asymptotic behavior, as the original field does not allow for infinite integration times. [FRT15] offer a finite-time solution to this problem: While relying on efficiently computable topological skeleton, a finite-time measure of separation is introduced that allows further investigation of the separatrices within the field.

In this work, we will deduce the connection between Vector Field Topology and LCS by proving that Vector Field Topology is Galilean invariant. To this end, we define *Path Line Topology* by observing steady vector fields in an unsteady reference frame and show that FTLE ridges and topological skeleton coincide therein. Furthermore, we extend the method to 3D vector fields, by applying a slightly adapted version of the separation measures to separatrix planes.

Notation

We will use the notation established in [FRT15]: Let $\mathbf{v}$ be a bounded steady vector field with Jacobian $\mathbf{J}$ and flow map $\phi(\mathbf{x},\tau)$. A stream line originating in $\mathbf{x}$ is a parametric curve $\phi(\mathbf{x},\tau)$. We will further utilize the normalized perpendicular field $\mathbf{w}(\mathbf{v})$. In the following chapter, we will give an overview over the separation measures introduced in [FRT15].

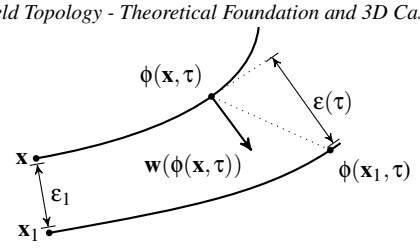

Figure 1: [FRT15] Construction of separation measure

Finite-Time Steady 2D Vector Field Topology

The separation at a given point in a vector field is described by the distance between two massless particles that were seeded infinitively close to each other. An overview of of the construction is given in figure 1: To compute the separation at position $\mathbf{x}$ on a stream line, a second particle is offset along the normal field $\mathbf{w}(\mathbf{x})$ to some $\mathbf{x}_1 = \mathbf{x} + \varepsilon_1 \mathbf{w}(\mathbf{x})$. The further these line move apart, the higher the separation. When we simplify the distance to its projection onto the normal, i.e., the component perpendicular to the flow

$$\varepsilon(\tau) = \mathbf{w}(\phi(\mathbf{x},\tau))^T (\phi(\mathbf{x}_1,\tau) - \phi(\mathbf{x},\tau)),$$

we can express the separation after integration time τ as

$$s(\mathbf{x},\tau) = \lim_{\varepsilon_1 \to 0} \ln \frac{\varepsilon(\tau)}{\varepsilon_1}\,. \tag{1}$$

It can be shown that for the initial offset ε_1 converging to 0, this separation measure can equivalently be expressed as

$$s(\mathbf{x},\tau) = \int_0^\tau \mathbf{w}(\phi)^T \mathbf{J}(\phi)\, \mathbf{w}(\phi)\, dr \tag{2}$$

with $\phi = \phi(\mathbf{x}, r)$. This approach resembles the localized FTLE introduced in [KPH*09].

As will be shown in section 3, we can reduce all computations to the topological skeleton of the field. Instead of a general stream line, τ now moves from a source towards a saddle (or backwards from sink to saddle) while the separation converges to a linear function

$$\lim_{\tau \to \infty} s(\mathbf{x},\tau) = a\,\tau + b(\mathbf{x}). \tag{3}$$

Here, a is the derivative in direction of the corresponding saddles eigenvector. We are particularly interested in $b(\mathbf{x})$: the difference between $s(\mathbf{x},\tau)$ to this final linear behavior. It becomes constant in the linear neighborhood of the saddle. An example can be seen in figure 2.

While $s(\mathbf{x},\tau)$ describes the perpendicular separation for integration towards the saddle, $b(\mathbf{x})$ captures the more expressive difference to the final linear behavior: The linear neighborhood of the saddle can easily be seen as the constant section. Lower values of $b(\mathbf{x})$ indicate asymptotically less separating areas and vice versa. As can be easily shown, $s(\mathbf{x},\tau)$ only differs by a translation at each point along the separatrix. For $b(\mathbf{x})$ follows:

Theorem 1 Given are two points $\mathbf{x}$, $\mathbf{y}$ on the same separatrix such that $\mathbf{y} = \phi(\mathbf{x},\tau_\mathbf{y})$. Then

$$b(\mathbf{y}) = b(\mathbf{x}) + s(\mathbf{x},\tau_\mathbf{y}) - a\,\tau_\mathbf{y}.$$

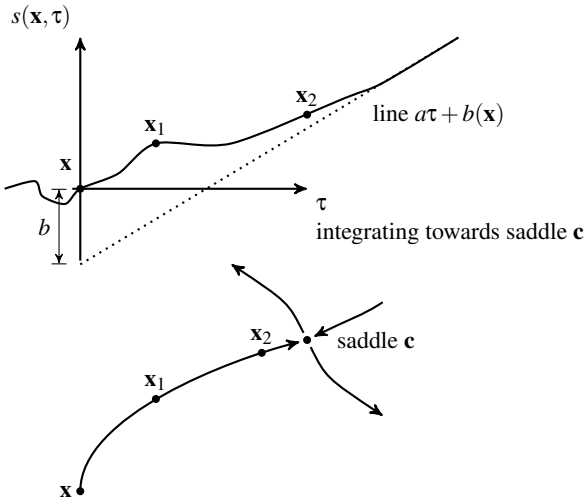

Figure 2: [FRT15] Behavior of $s(\mathbf{x},\tau)$ for a separatrix.

When integrating outwards from a saddle $\mathbf{c}$, the algorithm to evaluate $b(\mathbf{x})$ becomes rather simple:

- Compute a
- Start integration at a point $\mathbf{x}_0$ in the linear neighborhood of the saddle. This property can be easily verified.
- Starting with $b(\mathbf{c},0)=0$, integrate $b(\mathbf{c},\tau)$ by evaluating $s(\phi(\mathbf{c},\tau))$ locally. At each step, only local derivatives are used.
- Stop in the neighborhood of a source or sink.

To map this to a more visually expressive representation, we can introduce the function

$$h(\mathbf{x}) = a\, e^{k\,b(\mathbf{x})}.$$

In the linear neighborhood, $h(\mathbf{x})$ stays constant at a, making it possible to compare separation strengths of different separatrices. k is the only parameter needed throughout all computations. It steers the visual impact of deviations from the final separation.

An example of a small vector field is shown in figure 3 with all measures mentioned above.

3. On the relation of FTLE and Vector Field Topology for Steady Vector Fields

In this section, we study the relation of the two well-known concepts FTLE and Vector Field Topology in steady vector fields. The ridges will serve as the theoretical basis of our method.

For steady vector fields, both FTLE and Vector Field Topology (VFT) can be computed. Hence the question for their relation arises. In particular the relation of the limit of FTLE for an integration time converging to infinity and VFT is of interest since VFT captures the asymptotic behavior. It is known [Sad15] that FTLE and VFT sometimes show similar structures. Is is assumed that VFT is not Galilean invariant, and thus cannot coincide with FTLE. In fact, VFT heavily relies on the location and tracking of critical points. To illustrate this, [Sad15] shows an example of a changing topological skeleton after adding a constant vector field.

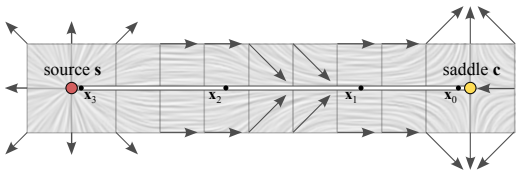

(a) Construction of a simple vector field on a 12×3 grid with a source, a saddle and a full separatrix in between. Velocity is interpolated bilinearly.

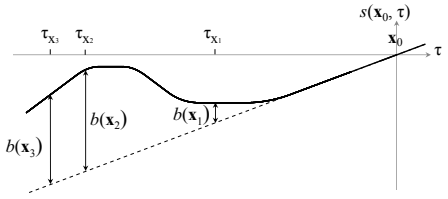

(b) Graph of $s(\mathbf{x},\tau)$. Note the differing spacing of $\mathbf{x}_0,\ldots,\mathbf{x}_3$ in space and over integration time τ.

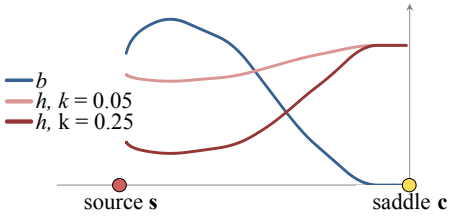

(c) Graphs of $b(\mathbf{x})$ and $h(\mathbf{x})$ for varying k. Larger values of k enhance deviations of $b(\mathbf{x})$ from 0.

Figure 3: [FRT15] $s(\mathbf{x},\tau)$, $b(\mathbf{x})$ and $h(\mathbf{x})$ on an example data set.

Here we introduce a slight modification of the concept of VFT. We use the fact that VFT aims at segmenting the flow in areas of similar asymptotic behavior, and that the extraction of critical points turns out to be the realization of this idea for studying the asymptotic behavior of stream lines. In our modification, we consider VFT as an approach to segmenting the *path lines* of a steady vector field into regions of similar asymptotic behavior (instead of stream lines that are usually related to VFT). We call this the *Path Line Topology (PLT)* of a steady vector field.

After a formal introduction, we show the following properties:

- Path Line Topology is Galilean invariant.
- For steady vector fields, Path Line Topology and Vector Field Topology coincide.
- For steady vector fields, separatrices starting from saddles in the Path Line Topology are FTLE ridges for integration times converging to infinity.

We stress again that we are interested in a topological segmentation of steady vector fields only. However, analyzing the Galilean invariance in a steady vector field $\mathbf{v}(\mathbf{x})$ requires the observation of $\mathbf{v}$ in a frame of reference moving with a constant speed: $\mathbf{x}' = \mathbf{x}+\mathbf{x}_0+t\mathbf{r}$ where $\mathbf{x}_0,\mathbf{r}$ are certain constants. The observation in such a moving frame transforms the *steady* vector field $\mathbf{v}(\mathbf{x})$ into an *unsteady* vector field $\mathbf{w}(\mathbf{x},t)=\mathbf{v}(\mathbf{x}')$. This means that for analyzing the Galilean invariance of steady VFT, we have to define VFT for unsteady vector fields as well. For this we have different choices as long as they

coincide with the classical VFT in the steady case. One such choice is the path line topology introduced below.

Note that observing $\mathbf{v}$ in a continuously moving frame of reference does *not* mean to add a constant field to $\mathbf{v}$. In fact, adding a constant vector field to $\mathbf{v}$ changes both the topological skeleton and FTLE and is therefore not directly related to Galilean invariance. (To be precise: invariance under adding a constant field is a sufficient but not necessary condition for Galilean invariance.)

Path line topology

Let $\mathbf{v}(\mathbf{x},t)$ be a 2D unsteady vector field, Jacobian $\mathbf{J}$ with non-vanishing determinant, and let

$$\mathbf{f_v} = \frac{1}{\det(\mathbf{J})}\begin{pmatrix}\det(\mathbf{v}_y,\mathbf{v}_t)\\ \det(\mathbf{v}_t,\mathbf{v}_x)\end{pmatrix} \tag{4}$$

be the 2D feature flow field [TS03]. Then we introduce path line topology by defining the new vector field

$$\hat{\mathbf{v}} = \mathbf{v} - \mathbf{f_v} \tag{5}$$

and analyze the topological skeleton of $\hat{\mathbf{v}}$ instead of $\mathbf{v}$: we extract and track the critical points of $\hat{\mathbf{v}}$, classify them by an eigenanalysis of the Jacobian $\hat{\mathbf{J}}$ of $\hat{\mathbf{v}}$, and integrate separatrices as path lines in $\hat{\mathbf{v}}$ starting from the saddles in $\hat{\mathbf{v}}$ in the direction of the eigenvectors of the Jacobian $\hat{\mathbf{J}}$ of $\hat{\mathbf{v}}$.

Properties of path line topology

In the following we restrict ourselves to the analysis of the critical points of path line topology instead of the complete topological skeleton. We show three things:

1. If $\mathbf{v}$ is steady, the critical points of $\mathbf{v}$ and $\hat{\mathbf{v}}$ coincide.
2. If a vector field $\mathbf{u}$ is obtained by observing a steady vector field $\mathbf{v}$ under a moving frame of reference, then $\mathbf{f_u} = \mathbf{r} = \text{const}$.
3. Critical points of $\hat{\mathbf{v}}$ are Galilean invariant.

Point 1 follows directly from the definition of $\hat{\mathbf{v}}$: if $\mathbf{v}$ is steady, we have $\mathbf{v}_t = \mathbf{0}$ which gives $\mathbf{f_v} = \mathbf{0}$. Point 2 can be shown by applying basic differentiation rules to $\mathbf{w}(\mathbf{x},t) = \mathbf{v}(\mathbf{x}+\mathbf{x}_0+t\mathbf{r})$. It has the following interpretation: $\mathbf{f_v}$ is a local estimator of the moving frame of reference. Point 3 follows from the relation

$$\mathbf{v} - \mathbf{f_v} = \mathbf{J}^{-1}\mathbf{a} \tag{6}$$

that was introduced in [GT15] (where $\mathbf{a} = \mathbf{J}\mathbf{v} + \mathbf{v}_t$ is the acceleration) and the well-known fact that both $\mathbf{J}$ and $\mathbf{a}$ are Galilean invariant.

FTLE in the limit

We assume a steady vector field $\mathbf{v}(\mathbf{x})$ with the following properties.

- $\mathbf{v}$ is bounded, i.e., $\|\mathbf{v}\|$ does not exceed a certain threshold.
- From every point of its domain, $\mathbf{v}$ can be (forward) integrated with an integration time converging to infinity, i.e. the particle does not leave the domain.

In particular, we expect a particle integration in $\mathbf{v}$ to either

- remain at its starting point $\mathbf{x}$ if $\mathbf{x}$ is a critical point, or
- converge towards a critical point with increasing integration time, or
- remain on an attracting closed orbit with increasing integration time.

These properties are rather common. Even when the domain is finite, no-slip boundaries often ensure that particles can not move outside.

Before analyzing the FTLE limits of $\mathbf{v}$, we study the FTLE behavior of a 2D linear vector field $\mathbf{v}_l$. Since in this case the Jacobian is constant, FTLE of $\mathbf{v}_l$ is constant for a fixed integration time τ. We are interested in the limit of FTLE for $\tau \to \infty$. Given is the linear vector field

$$\mathbf{v}_l = \mathbf{J}\mathbf{x} \tag{7}$$

with the constant Jacobian $\mathbf{J}$ that induces the flow map $\phi^\tau(\mathbf{x})$. Let λ_1, λ_2 be the eigenvalues of $\mathbf{J}$, and let $\mathbf{e}_1, \mathbf{e}_2$ be the corresponding eigenvectors. Furthermore, let $\mu_1(\tau), \mu_2(\tau)$ be the eigenvalues of the Cauchy-Green tensor $(\nabla\phi^\tau(\mathbf{x}))^T(\nabla\phi^\tau(\mathbf{x}))$. Then the following holds:

$$\lim_{\tau\to\infty}\left\{\frac{1}{\tau}\ln\sqrt{\mu_i(\tau)}\right\} = \{\mathrm{Re}(\lambda_i)\}\,. \tag{8}$$

(8) says that for a linear vector field, FTLE converges to the real part of the largest eigenvalue of $\mathbf{J}$ for increasing integration time. To show (8) , we use the fact that for a linear vector field (7) the flow map can be written in a closed form

$$\phi^\tau(\mathbf{x}) = \mathbf{E}\,\mathbf{D}\,\mathbf{E}^{-1}\,\mathbf{x} \tag{9}$$

with

$$\mathbf{E} = (\mathbf{e}_1, \mathbf{e}_2)\ ,\ \mathbf{D} = \begin{pmatrix} e^{\lambda_1\tau} & 0 \\ 0 & e^{\lambda_2\tau}\end{pmatrix}. \tag{10}$$

This gives also a simple closed form for the gradient:

$$\nabla\phi^\tau(\mathbf{x}) = \mathbf{E}\,\mathbf{D}\,\mathbf{E}^{-1}. \tag{11}$$

From this it is a straightforward exercise in algebra to show (8).

We now use (8) to analyze the general vector field $\mathbf{v}$. Suppose that $\mathbf{x}$ lies on a separatrix of $\mathbf{v}$, i.e., a forward integration from $\mathbf{x}$ converges to a saddle. Since from a certain time on the distance to the saddle decreases with exponential rate, we can assume that after a finite time the particle is within the linear neighborhood of the saddle – the region that is dominated by the first term of the Taylor expansion of $\mathbf{v}$ around the saddle [Gar07]. Then (8) gives that FTLE converges to the largest eigenvalue of the Jacobian at the saddle. This gives

$$\lim_{\tau\to\infty}\mathrm{FTLE}^\tau(\mathbf{x}) > 0 \text{ for } \mathbf{x} \text{ on a separatrix.} \tag{12}$$

If $\mathbf{x}$ is not on a separatrix but converges towards a sink, we use a similar argumentation: we use the fact that at a sink we have only negative real parts of the eigenvalues of the Jacobian and get

$$\lim_{\tau\to\infty}\mathrm{FTLE}^\tau(\mathbf{x}) < 0 \text{ for } \mathbf{x} \text{ concerging to a sink.} \tag{13}$$

Then (12), (13) give that separatrices are FTLE ridges for increasing integration times.

Remarks:

- Similar considerations can be made for $\mathbf{x}$ converging to an attracting closed orbit. Also in this case, FTLE converges to a negative value.
- Note that a linear vector field $\mathbf{v}$ is excluded from the considerations because it fails to be bounded. In fact, for a linear field, forward integration does not generally converge to a critical point or closed orbit.

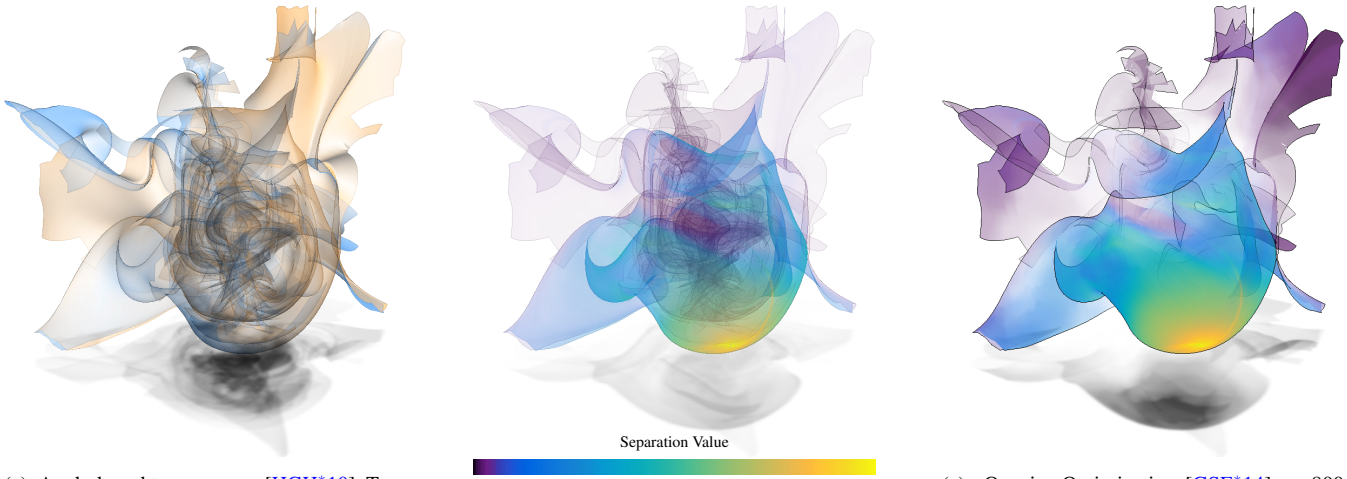

(a) Angle-based transparency [HGH*10], Two-Sided Shading, Layer Adaptivity [CFM*13] and silhouettes via depth discontinuities.

(b) Importance-based mapping. The colormap is tailored to the visible separation range. Opacity decreases linearly.

(c) Opacity Optimization [GSE*14] on 800 patches. Areas of high separation values and context are visually enhanced where possible.

Figure 4: Three different methods for visualizing separation on surfaces. Shadows are rendered using Fourier Opacity Mapping [JB10].

4. Extension to 3D Vector Fields

In the following, we will extend the method presented in [FRT15] to 3D vector fields. While the visualization differs, the computation of the separation values stays largely the same.

4.1. 3D Computation

When analyzing 3D fields, a few changes have to be made to account for the separatrices being surfaces instead of lines.

A stream surfaces is spanned by streamlines, here originating in a ring within the linear neighborhood of the saddle, and timelines in an advancing front. To integrate the surface we use a variant of the algorithm described in [Hul92]. We apply our method on each streamline starting or ending in the linear neighborhood of a saddle's separating plane, thus, along the flow. We measure the perpendicular separation along each separating surface. Therefore, we define the surface normal as perpendicular field $\mathbf{w}(\mathbf{x})$, and can compute values for $h(\mathbf{x})$ on each point on the separating surface.

Since Jacobian and normal are changing smoothly along the surface, it is sufficient to compute the separation for a finite number of streamline and interpolate in between. To insert a new streamline at places where the surface is diverging, the initial values of $h(\mathbf{x})$ can thus be interpolated from its neighbors, given that the resolution is high enough. Note that a, the initial separation, is constant on each separatrix, as it only depends on the common seed point.

4.2. 3D Visualization

Separating planes can form complex geometries that are difficult to visually comprehend. In figure 4 this can be seen as a single separtrix folds into itself with increasing integration time. Without rendering the surface transparent, these structures would not be visible. On this surface, separation strength is now visualized. We map h to a colormap and opacity. Dark colors and high opacity thereby mark regions of high separation.

Mapping to the vertex opacity and alpha blending makes it easier to determine regions of high separation: even parts hidden by geometry can be seen, as long as they have a high separation value and thus a high opacity. Still, highly important regions may stay unseen, especially when a high number of triangles overlaps at a pixel.

Three possible methods for mapping to color and opacity are shown in figure 4. The surface is the same as in figure 5. All shadows were rendered with Fourier Opacity Mapping by Jansen et al. [JB10].

In figure 4a, the surface is displayed applying angle-based transparency and two-sided shading as described in Hummel et al. [HGH*10]. Additionally, layer adaptivity by Carnecky et al. [CFM*13] and a depth-based silhouette extraction were applied to highlight the geometry folding. While this combination gives a good understanding of the surface geometry, the separation function is not encoded, as both color and transparency are used already.

In figure 4b, the computed separation values are encoded in both color and opacity. Areas of high separation are both highlighted by bright colors and high opacity. The geometry is still clearly visible, especially when animated as in the accompanying video. Regions of high separation are clearly visible from most angles, while less important areas fade out.

Finally, Opacity Optimization for surfaces by Günther et al. [GSE*14] was applied to the surface to highlight the regions of interest even more. This view-dependent technique balances feature highlighting and clutter removal: less important areas as at the borders and in the twisted middle are only visible when they do not visually occlude more important regions.

While Opacity Optimization yields the best results when animating the surface, it makes the geometry harder to understand. Therefore, in the remainder of this work surfaces will be displayed with the importance-based mapping. However, in an interactive application Opacity Optimization would be the preferable method.

Results

Borromean data set. Figure 5 visualizes the separating surface in one time slice of the Borromean dataset, simulated by Candelaresi and Brandenburg [CB11]. It contains the simulation of a magnetic field around Borromean rings. As opposed to figure 4b and 4c, the colormap in use encodes both separation strength and sign.

Benzene magnetic field. The Benzene dataset contains the normalized potential field of a benzene molecule [ZSH96]. Figure 6 shows the separatrices in the magnetic field around a benzene molecule. Separation is encoded in color and opacity. 124 saddle points and their respective separatrices are shown. This high number of surfaces would normally be infeasible to visualize. As we render areas of low separation transparent, the visual complexity is reduced since most surfaces disappear when their separation is low (compare to figure 6c for all surfaces). It shows that the main asymptotic separation happens around the outer hydrogen ring.

5. Discussion and Limitations

For the analysis of finite-time separation in steady fields, we have shown that the LCS coincide with the Vector Field Topology skeleton. By restricting the computation to the separatrices, we do not have to evaluate the field globally. Furthermore, in simplifying the separation measure to the perpendicular part only, the computation is reduced to the summation of directional derivatives along the line.

The computation of $s(\mathbf{x})$ depends on the initial distance ε_1 to the saddle at which the integration is started. As mentioned earlier, this problem can be resolved by forcing the seeding point to lay in its linear neighborhood.

The property displayed, $b(\mathbf{x})$, captures the difference of the asymptotic separation on the separatrix to the final linear behavior at the connected saddle. Within the linear neighborhood of the saddle, $b(\mathbf{x})$ is constant. This allows us to rely on finite integration times only to capture the asymptotic behavior: $b(\mathbf{x})$ is not a local property, but contains the accumulated perpendicular separation for particles seeded at $\mathbf{x}$ over a finite integration time.

For a more expressive visualization, $b(\mathbf{x})$ is scaled logarithmically in the displayed function $h(\mathbf{x})$. This introduces the only parameter: k steers the visual impact of deviations from the linear behavior. An example can be seen in figure 3c: While the functions differ in value, the behavior stays similar, leading to the same visual impression.

All examples given have a rather low number of critical points compared to measured and turbulent data. This is a common problem of topological methods: A more complicated topological skeleton will lead to occlusion and a cluttered visualization. Still, the high number of separatrices in the Benzene dataset (s. figure 6a) could be visualized well with mapping separation to opacity only.

In 3D datasets more problem occur for a high number of separatrices or surfaces folding back on themselves, as is the case in the Borromean dataset (s. figure 5b). Simple alpha blending in this case quickly results in a fully opaque image. Opacity Optimization [GSE*14] has been used to circumvent this problem. By linking opacity – and thus visibility – to the relative importance, regions of interest are highlighted, even when they lay inside other structures.

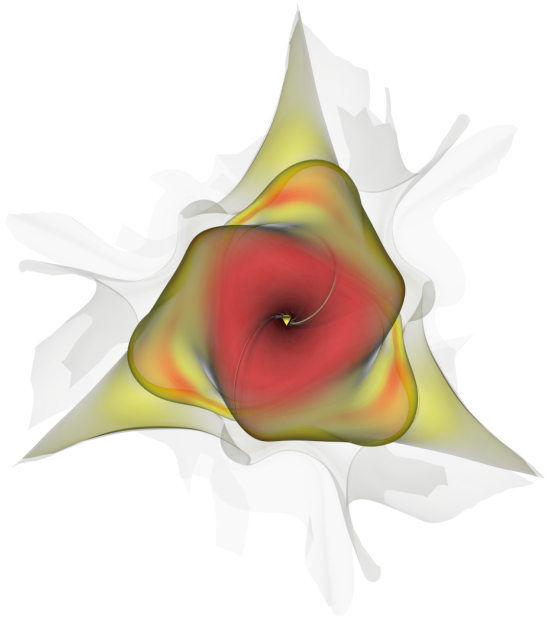

(a) The symmetry shown from the front.

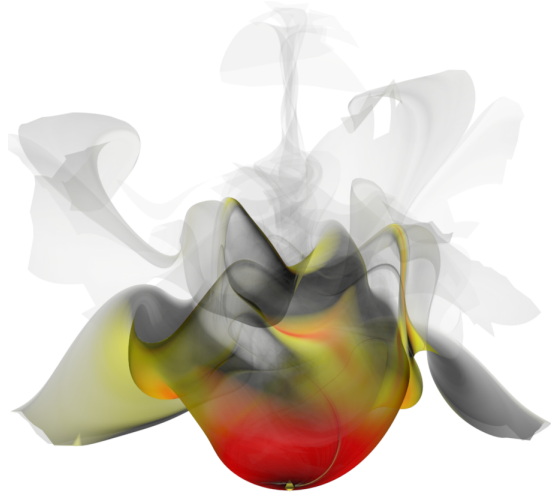

(b) Side view. The separation decreases from the saddle outwards.

Figure 5: Single separatrix surface in the Borromean dataset.

Future research

In general steady divergence-free vector fields, a separatrix connecting two saddles can occur. Changes in the computation of $b(\mathbf{x})$ might be sought to guarantee their sensible handling. Other topologically relevant structures that can be of interest are closed streamlines and boundary switch curves.

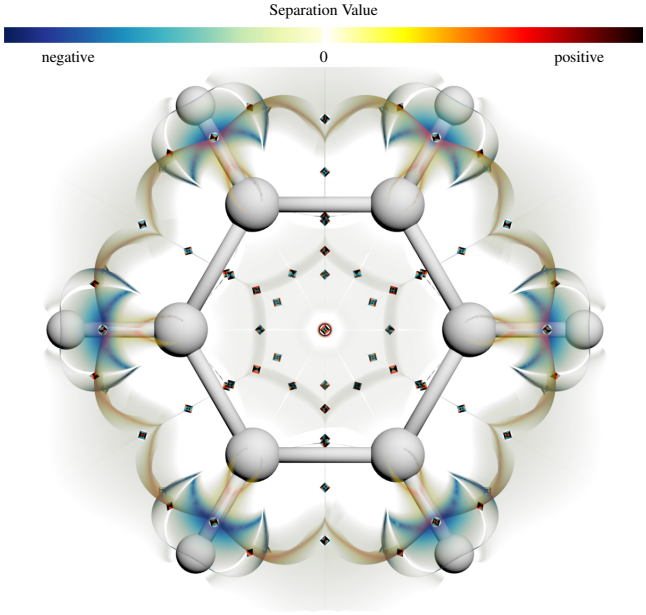

(a) Top View

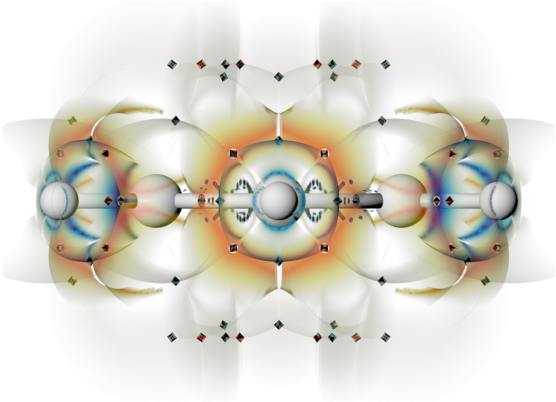

(b) Side View

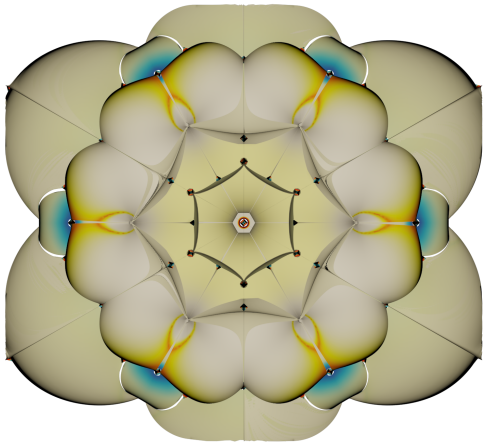

(c) Opaque Top View

Figure 6: Three views of a Benzene molecule. The atom structure is represented by the white mesh.

References

[BPKB14] BHATIA H., PASCUCCI V., KIRBY R. M., BREMER P.-T.: Extracting features from time-dependent vector fields using internal reference frames. *Computer Graphics Forum (Proc. EuroVis) 33*, 3 (June 2014), 21–30. 1, 2

[CB11] CANDELARESI S., BRANDENBURG A.: Decay of helical and nonhelical magnetic knots. *Physical Review E 84*, 1 (2011), 016406. 6

[CFM*13] CARNECKY R., FUCHS R., MEHL S., JANG Y., PEIKERT R.: Smart transparency for illustrative visualization of complex flow surfaces. *IEEE Transactions on Visualization and Computer Graphics 19*, 5 (2013), 838–851. 5

[dLvL99a] DE LEEUW W., VAN LIERE R.: Collapsing flow topology using area metrics. In *Proc. IEEE Visualization '99* (1999), pp. 149–354. 1, 2

[dLvL99b] DE LEEUW W., VAN LIERE R.: Visualization of global flow structures using multiple levels of topology. In *Data Visualization 1999. Proc. VisSym 99* (1999), pp. 45–52. 2

[FRT15] FRIEDERICI A., RÖSSL C., THEISEL H.: Finite time steady 2D vector field topology. In *Proc. Topo-In-Vis 2015* (Annweiler, Germany, May 20-22 2015). 1, 2, 3, 5

[Gar07] GARTH C.: *Visualization of complex three-dimensional flow structures.* PhD thesis, University of Kaiserslautern, 2007. 4

[GGSLHH09] GARTH C., GUO-SHI LI X. T., HANSEN C. D., HAGEN H.: Visualization of coherent structures in transient 2D flows. In *Proceedings of TopoInVis 2007* (2009), pp. 1–13. 2

[GGTH07] GARTH C., GERHARDT F., TRICOCHE X., HAGEN H.: Efficient computation and visualization of coherent structures in fluid flow applications. *IEEE Transactions on Visualization and Computer Graphics 13*, 6 (2007), 1464–1471. 2

[GKT16] GÜNTHER T., KUHN A., THEISEL H.: MCFTLE: Monte Carlo rendering of finite-time Lyapunov exponent fields. *Computer Graphics Forum (Proc. EuroVis) 35*, 3 (2016), 381–390. 2

[GLL91] GLOBUS A., LEVIT C., LASINSKI T. A.: A tool for visualizing the topology of three-dimensional vector fields. In *Proc. IEEE Visualization* (1991), pp. 33–40. 2

[GSE*14] GÜNTHER T., SCHULZE M., ESTURO J. M., RÖSSL C., THEISEL H.: Opacity optimization for surfaces. In *Computer Graphics Forum* (2014), vol. 33, pp. 11–20. 5, 6

[GT15] GÜNTHER T., THEISEL H.: Finite-time mass separation for comparative visualizations of inertial particles. *Computer Graphics Forum (Proc. EuroVis) 34*, 3 (2015), 471–480. 4

[Hal01] HALLER G.: Distinguished material surfaces and coherent structures in three-dimensional fluid flows. *Physica D 149* (2001), 248–277. 2

[Hal02] HALLER G.: Lagrangian coherent structures from approximate velocity data. *Physics of Fluids 14*, 6 (2002). 2

[HGH*10] HUMMEL M., GARTH C., HAMANN B., HAGEN H., JOY K. I.: IRIS: Illustrative rendering for integral surfaces. *IEEE Transactions on Visualization and Computer Graphics 16*, 6 (2010), 1319–1328. 5

[HH89] HELMAN J. L., HESSELINK L.: Representation and display of vector field topology in fluid flow data sets. *IEEE Computer 22*, 8 (1989), 27–36. 1

[HH91] HELMAN J. L., HESSELINK L.: Visualizing vector field topology in fluid flows. *IEEE Computer Graphics and Applications 11* (1991), 36–46. 2

[HLH*16] HEINE C., LEITTE H., HLAWITSCHKA M., IURICICH F., DE FLORIANI L., SCHEUERMANN G., HAGEN H., GARTH C.: A survey of topology-based methods in visualization. In *Computer Graphics Forum* (2016), vol. 35, Wiley Online Library, pp. 643–667. 2

[Hul92] HULTQUIST J. P. M.: Constructing stream surfaces in steady 3D vector fields. In *Proceedings of the 3rd conference on Visualization'92* (1992), IEEE Computer Society Press, pp. 171–178. 5

[HY00] HALLER G., YUAN G.-C.: Lagrangian coherent structures and mixing in two-dimensional turbulence. *Physica D 147*, 3-4 (2000), 352–370. 2

[JB10] JANSEN J., BAVOIL L.: Fourier opacity mapping. In *Proceedings of the 2010 ACM SIGGRAPH symposium on Interactive 3D Graphics and Games* (2010), ACM, pp. 165–172. 5

[KPH*09] KASTEN J., PETZ C., HOTZ I., NOACK B. R., HEGE H.-C.: Localized finite-time Lyapunov exponent for unsteady flow analysis. In *Vision Modeling and Visualization* (2009), pp. 265 – 274. 2

[LCM*05] LEKIEN F., COULLIETTE C., MARIANO A. J., RYAN E. H., SHAY L. K., HALLER G., MARSDEN J.: Pollution release tied to invariant manifolds: A case study for the coast of Florida. *Physica D 210*, 1 (2005), 1–20. 2

[LHZP07] LARAMEE R. S., HAUSER H., ZHAO L., POST F. H.: Topology-based flow visualization, the state of the art. In *Topology-based Methods in Visualization*, Hauser H., Hagen H., Theisel H., (Eds.), Mathematics and Visualization, 2007, pp. 1–19. 2

[LM10] LIPINSKI D., MOHSENI K.: A ridge tracking algorithm and error estimate for efficient computation of Lagrangian coherent structures. *Chaos: An Interdisciplinary Journal of Nonlinear Science 20*, 1 (2010), 017504. 2

[LRR00] LODHA S. K., RENTERIA J. C., ROSKIN K. M.: Topology preserving compression of 2D vector fields. In *Proc. IEEE Visualization* (2000), pp. 343–350. 2

[MBHJ03] MAHROUS K. M., BENNETT J. C., HAMANN B., JOY K. I.: Improving topological segmentation of three-dimensional vector fields. In *Data Visualization (Proc. VisSym)* (2003), pp. 203–212. 2

[MBS*04] MAHROUS K. M., BENNETT J. C., SCHEUERMANN G., HAMANN B., JOY K. I.: Topological segmentation in three-dimensional vector fields. *IEEE Transactions on Visualization and Computer Graphics 10*, 2 (2004), 198–205. 2

[PPF*11] POBITZER A., PEIKERT R., FUCHS R., SCHINDLER B., KUHN A., THEISEL H., MATKOVIC K., HAUSER H.: The state of the art in topology-based visualization of unsteady flow. *Computer Graphics Forum 30*, 6 (2011), 1789–1811. 2

[PPF*12] POBITZER A., PEIKERT R., FUCHS R., THEISEL H., HAUSER H.: Filtering of FTLE for visualizing spatial separation in unsteady 3D flow. In *Topological Methods in Data Analysis and Visualization II*, 2012, pp. 237–253. 2

[Sad15] SADLO F.: Lyapunov time for 2D Lagrangian visualization. In *Topological and Statistical Methods for Complex Data*, 2015, pp. 167–181. 3

[SKMR98] SCHEUERMANN G., KRÜGER H., MENZEL M., ROCKWOOD A. P.: Visualizing non-linear vector field topology. *IEEE Transactions on Visualization and Computer Graphics 4*, 2 (1998), 109–116. 1

[SLM05] SHADDEN S. C., LEKIEN F., MARSDEN J. E.: Definition and properties of Lagrangian coherent structures from finite-time Lyapunov exponents in two-dimensional aperiodic flows. *Physica D 212*, 7 (2005), 271–304. 2

[SLP*09] SHADDEN S. C., LEKIEN F., PADUAN J. D., CHAVEZ F. P., MARSDEN J. E.: The correlation between surface drifters and coherent structures based on high-frequency radar data in Monterey Bay. *Deep Sea Research Part II: Topical Studies in Oceanography 56*, 3-5 (2009), 161–172. 2

[SLR03] SURESH LODHA N. M. F., RENTERIA J. C.: Topology preserving top-down compression of 2D vector fields using bintree and triangular quadtrees. *IEEE Transactions on Visualization and Computer Graphics 9*, 4 (2003), 433–442. 2

[SP07] SADLO F., PEIKERT R.: Efficient visualization of Lagrangian coherent structures by filtered AMR ridge extraction. *IEEE Transactions on Visualization and Computer Graphics (Proceedings Visualization) 13*, 6 (2007), 1456–1463. 2

[SP09] SADLO F., PEIKERT R.: Visualizing Lagrangian coherent structures and comparison to vector field topology. In *Proceedings of TopoInVis 2007* (2009), pp. 15–30. 2

[SRP11] SADLO F., RIGAZZI A., PEIKERT R.: Time-Dependent Visualization of Lagrangian Coherent Structures by Grid Advection. In *Proceedings of TopoInVis 2009* (2011), pp. 151–165. 2

[SW10] SADLO F., WEISKOPF D.: Time-Dependent 2D Vector Field Topology: An Approach Inspired by Lagrangian Coherent Structures. *Computer Graphics Forum 29*, 1 (2010), 88–100. 2

[The02] THEISEL H.: Designing 2D vector fields of arbitrary topology. *Computer Graphics Forum (Eurographics 2002) 21*, 3 (2002), 595–604. 2

[TRS03] THEISEL H., RÖSSL C., SEIDEL H.-P.: Compression of 2D vector fields under guaranteed topology preservation. *Computer Graphics Forum (Eurographics 2003) 22*, 3 (2003), 333–342. 2

[TS03] THEISEL H., SEIDEL H.-P.: Feature flow field. In *Proceedings of the symposium on Data visualisation* (2003), vol. 2003. 4

[TSH00] TRICOCHE X., SCHEUERMANN G., HAGEN H.: A topology simplification method for 2D vector fields. In *Proc. IEEE Visualization* (2000), pp. 359–366. 2

[TSH01] TRICOCHE X., SCHEUERMANN G., HAGEN H.: Continuous topology simplification of planar vector fields. In *Proc. IEEE Visualization* (2001), pp. 159 – 166. 2

[TWHS03] THEISEL H., WEINKAUF T., HEGE H.-C., SEIDEL H.-P.: Saddle connectors - an approach to visualizing the topological skeleton of complex 3D vector fields. In *Proc. IEEE Visualization 2003* (2003), pp. 225–232. 2

[USE13] UFFINGER M., SADLO F., ERTL T.: A time-dependent vector field topology based on streak surfaces. *IEEE Transactions on Visualization and Computer Graphics 19*, 3 (2013), 379–392. 2

[WGS07] WIEBEL A., GARTH C., SCHEUERMANN G.: Computation of localized flow for steady and unsteady vector fields and its applications. *IEEE Transactions on Visualization and Computer Graphics 13*, 4 (2007), 641–651. 1, 2

[WJE01] WESTERMANN R., JOHNSON C., ERTL T.: Topology-preserving smoothing of vector fields. *IEEE Transactions on Visualization and Computer Graphics 7*, 3 (2001), 222–229. 2

[WPJ*08] WELDON M. J., PEACOCK T. M., JACOBS G., HELU M., HALLER G.: Experimental and numerical investigation of the kinematic theory of unsteady separation. *Journal of Fluid Mechanics 611* (2008). 2

[WS01] WISCHGOLL T., SCHEUERMANN G.: Detection and visualization of closed streamlines in planar flows. *IEEE Transactions on Visualization and Computer Graphics 7*, 2 (2001), 165–172. 1

[WTHS04a] WEINKAUF T., THEISEL H., HEGE H.-C., SEIDEL H.-P.: Boundary switch connectors for topological visualization of complex 3D vector fields. In *Data Visualization (Proc. VisSym)* (2004), pp. 183–192. 2

[WTHS04b] WEINKAUF T., THEISEL H., HEGE H.-C., SEIDEL H.-P.: Topological construction and visualization of higher order 3D vector fields. *Computer Graphics Forum (Proc. Eurographics) 23*, 3 (2004), 469–478. 2

[WWL16] WANG W., WANG W., LI S.: From numerics to combinatorics: a survey of topological methods for vector field visualization. *Journal of Visualization* (2016), 1–26. 2

[ZSH96] ZOCKLER M., STALLING D., HEGE H.-C.: Interactive visualization of 3d-vector fields using illuminated stream lines. In *Visualization'96. Proceedings.* (1996), IEEE, pp. 107–113. 6